





Cite this: *RSC Adv.*, 2020, 10, 43312

# First-principles calculations of an asymmetric MoO<sub>2</sub>/graphene nanocomposite as the anode material for lithium-ion batteries†

Qiuyu Zhang,  Dongyang Zhu, Xiaowei Li \* and Yihe Zhang 

Previous work on the synthesis and preparation of MoO<sub>2</sub>/graphene nanocomposites (MoO<sub>2</sub>/G) indicates that MoO<sub>2</sub>/G is a good anode material for lithium-ion batteries (LIBS). In this work, we used larger super-cells than those used previously to theoretically construct an asymmetric MoO<sub>2</sub>/G nanocomposite with smaller lattice mismatch. We then calculated the structural, electronic and Li atom diffusion properties of MoO<sub>2</sub>/G using first-principles calculations based on density functional theory. The results show that asymmetric MoO<sub>2</sub>/G has metallic properties, good stability and a low Li atom diffusion barrier because of the charge transfer induced by van der Waals interactions. The Li diffusion barriers in the interlayer of MoO<sub>2</sub>/G are in the range of 0.02–0.29 eV, depending on the relative positions of the Li atom and the MoO<sub>2</sub> and the C atoms in the graphene layer. The Li diffusion barriers on the outside layers of the MoO<sub>2</sub>/G nanocomposite are smaller than those of its pristine materials (MoO<sub>2</sub> and graphene). These results are consistent with experimental results. The adsorption of Li atoms in the interlayer of the nanocomposite further promotes the adsorption of Li atoms on the outside sites of the MoO<sub>2</sub> layer. Hence, the specific capacity of the MoO<sub>2</sub>/G nanocomposite is larger than 1682 mA h g<sup>−1</sup>. These properties all indicate that MoO<sub>2</sub>/G is a good anode material for LIBS.

Received 8th September 2020  
Accepted 10th November 2020

DOI: 10.1039/d0ra07690b

rsc.li/rsc-advances

## 1. Introduction

Lithium-ion batteries (LIBS) are widely used as portable batteries in mobile phones, notebook computers, and electric vehicles, due to their high energy density, long life and good cycle performance.<sup>1–4</sup> The performance of LIBS is largely determined by the electrode materials used; traditional commercial LIBS mainly use lower-cost graphene as the anode material. However, its theoretical capacity is only 372 mA h g<sup>−1</sup>,<sup>5,6</sup> which cannot meet the high-capacity demand of lithium-ion batteries. In order to obtain a higher lithium storage capacity, transition metal oxides, such as TiO<sub>2</sub>, Fe<sub>3</sub>O<sub>4</sub>, Co<sub>3</sub>O<sub>4</sub>, MoO<sub>2</sub>, Fe<sub>2</sub>O<sub>3</sub>, SnO<sub>2</sub> and NiO, may be used as they have high theoretical capacities, rate performance, may be recycled and are low cost. Of these, MoO<sub>2</sub> stands out because of its good conductivity and high theoretical capacity of 838 mA h g<sup>−1</sup>, which is about 2.3 times that of graphene.<sup>7</sup> However, MoO<sub>2</sub> also has its significant disadvantages, for example, it experiences significant volume expansion and severe particle agglomeration during lithium atom insertion and extraction. This causes pulverization of the

MoO<sub>2</sub> powder, resulting in detachment of the electrode material and a rapid drop in capacity.<sup>8</sup> There are two methods that can be used to improve the above problems. One is to prepare nano-structured MoO<sub>2</sub>, such as nanoparticles, nanospheres, nanobelts or nanowires.<sup>9–11</sup> Compared to the bulk material, the nanomaterials have a larger ion contact area, are able to achieve high specific capacities and have shorter diffusion paths, which facilitates rapid diffusion and a high utilization of lithium ions. Another method is to form a composite of MoO<sub>2</sub> and carbon, thereby slowing or solving the problem of volume expansion caused by lithium ion insertion and extraction.<sup>7</sup>

Graphene is a two-dimensional planar sheet that exhibits sp<sup>2</sup> bonding, has a specific atomic thickness, a high specific surface area, good room temperature carrier mobility and thermal conductivity. Therefore, graphene is a very suitable material for the formation of composites of MoO<sub>2</sub> and carbon. In recent years, the preparation of MoO<sub>2</sub>/graphene (MoO<sub>2</sub>/G) nanocomposites and their properties have been investigated. Akkisetty Bhaskar<sup>12</sup> used non-toxic citric acid and polyethylene glycol to reduce graphene oxide and synthesize a MoO<sub>2</sub>/G composite under conditions limiting graphene and MoO<sub>2</sub> formation, thereby increasing the storage capacity and conductivity of the lithium atoms. Tang<sup>4</sup> used ascorbic acid as a reducing agent to form MoO<sub>2</sub> nanoparticles on graphene sheets via a two-step hydrothermal calcination to form a MoO<sub>2</sub>/G nanocomposite. The MoO<sub>2</sub> particles were dispersed on the graphene to change the MoO<sub>2</sub>/G composite into an amorphous

National Laboratory of Mineral Materials, Beijing Key Laboratory of Materials Utilization of Nonmetallic Minerals and Solid Wastes, School of Materials Science and Technology, China University of Geosciences (Beijing), Beijing 100083, China. E-mail: lixiaowei@cugb.edu.cn

† Electronic supplementary information (ESI) available. See DOI: 10.1039/d0ra07690b



structure, thereby expanding the lithium atom capacity, reducing the charge transfer resistance and the aggregation of the graphene sheets.

Theoretical studies can observe and analyze the stability and electrochemical properties of materials, such as the lithium adsorption capacity, the stability and the electrical conductivity of the material, from the atomic level. Recently, Jiachen Ma<sup>13</sup> used a smaller super-cell to theoretically construct a MoO<sub>2</sub>/G nanocomposite. It was found that the C–C bond length in the structure changed too much and the tensile strain was as high as 12%. However, these properties are difficult to achieve in an actual preparation process. Thus, in this work, *via* first-principles calculations based on density functional theory (DFT), we chose larger super-cells of MoO<sub>2</sub> and graphene to construct a MoO<sub>2</sub>/G nanocomposite with smaller lattice mismatch. We then studied the geometric stability, electronic properties, and the Li atom adsorption and diffusion properties of the MoO<sub>2</sub>/G nanocomposite.

## 2. Calculation methods

All the calculations were carried out using DFT as implemented in the Vienna *ab initio* simulation package (VASP).<sup>14</sup> The electronic exchange-correlation interaction was treated using the generalized gradient approximation (GGA) and the Perdew–Burke–Ernzerhof (PBE) functional.<sup>15</sup> The electronic wave function was extended in the plane wave basis set and used a kinetic energy cutoff of 500 eV. K-point sampling in the Brillouin area used the Monkhorst–Pack method. The minimum density of the point was  $2\pi \times 0.04 \text{ \AA}^{-1}$ . The convergences of energy and force were set as  $1 \times 10^{-5}$  eV,  $0.04 \text{ eV \AA}^{-1}$ . In the two-dimensional structural model, a 15 Å vacuum layer was placed in the non-periodic direction to ensure that there was no interaction between the periodic mirrors in this direction. To study the diffusion of Li in the nanocomposite, the nudged elastic band (NEB) method for determining the minimum energy path and energy barrier was implemented in VASP.<sup>16</sup>

## 3. Results and discussion

### 3.1 Structure

Because of the different lattice parameters of MoO<sub>2</sub> and graphene, we constructed the asymmetric MoO<sub>2</sub>/G nanocomposite using a  $6 \times 6$  graphene super-cell to match a  $5 \times 5$  MoO<sub>2</sub> super-cell. After structural optimization without any constraint, we found that the lattice mismatch was only 0.74%. As shown in Fig. 1a, we chose to assess four nanocomposites formed by varying the positions of the C atoms in graphene relative to the MoO<sub>2</sub> layer. These nanocomposites were named T<sub>1</sub>, T<sub>2</sub>, H and B and describe the situation where one C atom in graphene is located directly above either the O atom, the Mo atom, a hollow site or a bridge site of MoO<sub>2</sub>, respectively. In order to determine the most stable structure, we calculated the binding energies of the four structures. The binding energy  $E_b$  was calculated using the following formula:<sup>17</sup>

$$E_b = (E_{\text{MoO}_2} + E_G - E_{\text{MoO}_2/\text{G}})$$

where  $E_{\text{MoO}_2}$ ,  $E_G$ , and  $E_{\text{MoO}_2/\text{G}}$  are the energies of MoO<sub>2</sub>, graphene, and MoO<sub>2</sub>/G, respectively.

The calculated binding energies of nanocomposites T<sub>1</sub>, T<sub>2</sub>, H and B are 0.485, 0.503, 0.536, and 0.502 eV, respectively. Thus, we find that nanocomposite H is the most stable structure, the optimized structure of which is shown in Fig. 1b. The top view of the MoO<sub>2</sub>/G nanocomposite presents a hexagonal structure and the side view shows that the C atoms in the graphene layer are not strictly in plane. The distance between the graphene and MoO<sub>2</sub> layers varies depending by which MoO<sub>2</sub> site the C atom in graphene is located. The smallest distance is about 2.768 Å corresponding to the C atom located on the hollow site of MoO<sub>2</sub>, while the largest distance is about 3.111 Å corresponding to the C atom located on top of the O atom in MoO<sub>2</sub>. For the most stable MoO<sub>2</sub>/G nanocomposite, the calculated O–Mo bond length, O–O distance and O–Mo–O bond angle were about 2.068–2.070 Å, 2.424–2.906 Å, and 71.635–89.194°, which are slightly different from the results obtained for pristine MoO<sub>2</sub> (2.05 Å, 2.47 Å and 87.4°).<sup>18,19</sup> The calculated C–C bond length and C–C–C bond angle were about 1.395–1.404 Å and 119.87–120.135°, which are almost no different from the results seen in pristine graphene (1.426 Å and 120°). This is because of the unmatched lattice parameters and the interaction between graphene and MoO<sub>2</sub> during the construction of the nanocomposite.

### 3.2 Adsorption properties

The adsorption capacity is one of the main properties used to evaluate the performance of lithium electrode materials. In order to obtain the adsorption properties of Li atoms at different sites, we calculated the adsorption energy ( $E_{\text{ad}}$ ) which is defined as:<sup>20</sup>

$$E_{\text{ad}} = (E_{\text{MoO}_2/\text{G}+n\text{Li}} - E_{\text{MoO}_2/\text{G}} - nE_{\text{Li}})/n$$

where  $E_{\text{MoO}_2/\text{G}+n\text{Li}}$  and  $E_{\text{MoO}_2/\text{G}}$  are the energies of MoO<sub>2</sub>/G with and without Li atoms adsorbed.  $E_{\text{Li}}$  is the energy of the Li atom from its bulk structure, and  $n$  is the number of Li atoms.

For a low Li adsorption scenario, we model one Li adsorption in one super-cell. There are three adsorption layers, namely the interlayer between MoO<sub>2</sub> and graphene (MoO<sub>2</sub>/Li/G), the outside of the MoO<sub>2</sub> layer (Li/MoO<sub>2</sub>/G) and the outside of the graphene layer (MoO<sub>2</sub>/G/Li). Considering that the adsorption energy of Li on MoO<sub>2</sub> is larger than that on graphene, Li is prone to adsorb on the surface of the MoO<sub>2</sub> layer in the MoO<sub>2</sub>/G interlayer. For the adsorption on the surface of MoO<sub>2</sub>, on both the outside and the interlayer, four kinds of adsorption sites are considered. These are one hollow site, two top sites and one bridge site. For the adsorption on the outside of graphene, there are three adsorption sites, the hollow site of the carbon ring, on top of a C atom and on a bridge site of a C–C bond. The possible adsorption sites are shown in Fig. 1c.

The more negative the adsorption energy, the more stable the structure is. The calculated adsorption energies are tabulated in Table 1. Of the three adsorption layers, the interlayer adsorption is more favorable. The absolute values of the adsorption energies follow the following trend MoO<sub>2</sub>/Li/G > Li/



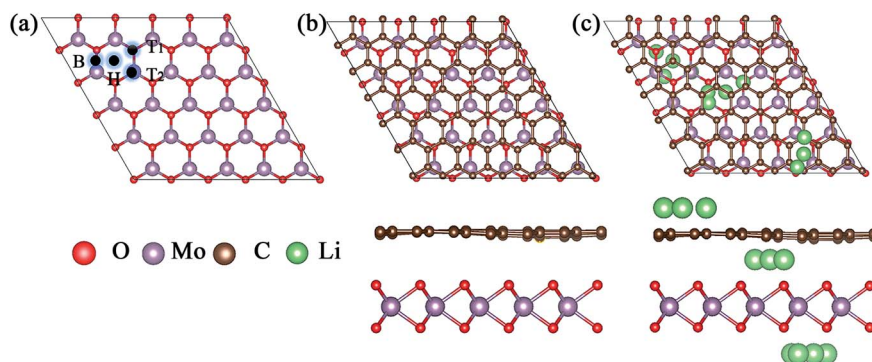


**Fig. 1** (a) The top view of  $\text{MoO}_2$ . B, H,  $T_1$  and  $T_2$  represent graphene carbon atoms located on bridge, hollow, O and Mo sites of  $\text{MoO}_2$ , respectively. (b) and (c) Top and side views of the optimized geometric structure of the  $\text{MoO}_2/\text{G}$  nanocomposite and the possible adsorption positions for Li atoms.

**Table 1** Calculated adsorption energies of Li atoms ( $E_{\text{ad}}$ ) on different hollow sites and the interlayer distance ( $d$ ) between  $\text{MoO}_2$  and graphene

Structure	$E_{\text{ad}}$ (eV)	$d$ (Å)
$\text{MoO}_2/\text{G}$	—	2.768–3.111
$\text{MoO}_2/\text{Li}/\text{G}$	−2.358 to −2.040	2.708–3.151
$\text{Li}/\text{MoO}_2/\text{G}$	−1.913 to −1.917	2.745–3.101
$\text{MoO}_2/\text{G}/\text{Li}$	−1.013 to −0.989	2.711–3.083

$\text{MoO}_2/\text{G} > \text{MoO}_2/\text{G}/\text{Li}$ . However, the most stable adsorption site for different layers is the hollow site of a  $\text{MoO}_2$  or graphene carbon ring. It is worth noting that the Li atom adsorbed on the bridge site will move to its nearest hollow site after structural optimization. The calculated adsorption energies of  $\text{MoO}_2/\text{Li}/\text{G}$  are in the range of −2.358 to −2.040 eV, depending on the relative positions of the C atoms and  $\text{MoO}_2$ , which meets the requirements of an anode material for Li-ion batteries.<sup>21</sup> As shown in Fig. 2, when one Li atom is adsorbed on pristine  $\text{MoO}_2$  the adsorption energy is −1.77 eV, which is larger than the adsorption energies of a Li atom in the interlayer. Therefore, the  $\text{MoO}_2/\text{G}$  nanocomposite is conducive to the adsorption of Li atoms. Unexpectedly, when a Li atom is adsorbed on the outside of the graphene layer (the  $\text{MoO}_2/\text{G}/\text{Li}$  structure), the calculated adsorption energy is negative, which is opposite to that of pristine graphene. The calculated adsorption energy of one Li on pristine graphene is 0.73 eV, which is slightly higher than the result reported by Das (0.71 eV).<sup>22</sup> To analyze the mechanisms giving rise to the adsorption energy, we calculated the adsorption energy of a Li atom on pristine graphene using a lattice parameter similar to the nanocomposite. The calculated result demonstrates that the adsorption energy is also positive. So, we can conclude that van der Waals interactions between  $\text{MoO}_2$  and graphene will promote the adsorption of Li atoms on the surface of graphene. Additionally, the adsorption of a Li atom on the outside of the  $\text{MoO}_2/\text{G}$  nanocomposite slightly reduces the interlayer distance, as shown in Table 1. Moreover, compared with the results found for the symmetric  $\text{MoO}_2/\text{G}$  nanocomposites constructed by Ma,<sup>13</sup> the asymmetric structure

is more favorable for the adsorption of Li atoms on the surface of graphene. To further verify the adsorption performance of Li atoms on  $\text{MoO}_2/\text{G}$ , a HSE06 functional was used to calculate the adsorption energies of one Li atom at the two outside sites and at the  $\text{MoO}_2/\text{G}$  interlayer. For the most favorable adsorption sites at the two outside sites and at the interlayer, the calculated adsorption energies are −1.447, −2.171 and −0.049 eV, respectively. This result further demonstrates that the asymmetric structure of  $\text{MoO}_2/\text{G}$  with smaller lattice mismatch will improve the adsorption performance of the material with respect to Li atoms.

Due to the lattice mismatch between  $\text{MoO}_2$  and graphene, we calculated the adsorption energies of one Li atom at different hollow sites of the  $\text{MoO}_2$  in the interlayer. As shown in Fig. 2a, there are 25 ( $5 \times 5$ ) hollow  $\text{MoO}_2$  adsorption sites in one supercell, namely coordinates 1 to 5 along the x and y axis. The calculated adsorption energies are shown in Fig. 2b. We can see that a Li atom has a larger adsorption energy (−2.358 eV) at the

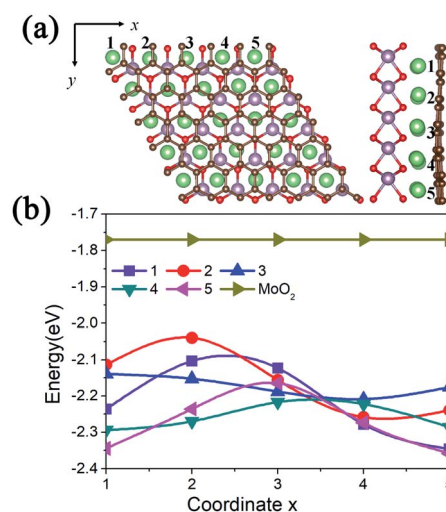


**Fig. 2** (a) Top and side views of the geometric structure of a Li atom at different hollow sites in the interlayer of  $\text{MoO}_2/\text{G}$ . (b) Adsorption energies of one Li atom in the interlayer of  $\text{MoO}_2/\text{G}$  and on the surface of pristine  $\text{MoO}_2$ .



site where the MoO<sub>2</sub> ring overlaps with the carbon ring of graphene (coordinate (5,5) in Fig. 2a), while it has smaller adsorption energy (−2.040 eV) at the site where the MoO<sub>2</sub> ring overlaps with the C atom of graphene (coordinate (2,2) in Fig. 2a). We also find that the lower the adsorption energy of the Li atom, the further away the C atom is from the center of the MoO<sub>2</sub> ring, this result is consistent with that of the mechanical analysis.

For a high Li atom adsorption scenario, we calculated multi-layer adsorptions as shown in Fig. 3 and Fig. 4. Due to larger adsorption energies in the interlayer, the first-layer of Li atoms are adsorbed in the MoO<sub>2</sub>/G interlayer with a calculated average Li atom adsorption energy of −1.256 eV. In order to verify the effect of interlayer adsorption on the adsorption at MoO<sub>2</sub> and graphene outside sites, we undertook the following experiments. If we only adsorbed one layer of Li atoms on the outside of the MoO<sub>2</sub> layer, the calculated average adsorption energy was −0.785 eV, as shown in Fig. 3a. This is obviously different from the value obtained for the second-layer Li adsorption on the outside of the MoO<sub>2</sub> layer (−1.426 eV), as shown in Fig. 3c. When we adsorbed only one layer of Li atoms on the outside of the graphene layer, the calculated average adsorption energy was 0.374 eV, as shown in Fig. 3b. This is slightly larger than the value obtained for the second-layer Li adsorption on the outside of the graphene layer (0.323 eV), as shown in Fig. 3d. Therefore, it can be concluded that the interlayer adsorption of Li atoms will largely promote the adsorption of Li atoms on the outside sites of both the MoO<sub>2</sub> layer and the graphene layer.

In order to further verify the stability of Li adsorption on the outside and in the interlayer of the MoO<sub>2</sub>/G nanocomposite, *ab initio* molecular dynamics (AIMD) simulations

were carried out for the adsorption of three layers at 300 K, and the results are shown in Fig. S1.† It can be seen that after 5 ps Li atoms were adsorbed well on both the surface of the MoO<sub>2</sub> layer and in the interlayer of the MoO<sub>2</sub>/G nanocomposite, and that only some of the Li atoms on the outside sites of the graphene layer were separated from their original positions. The AIMD results are consistent with the adsorption energies calculated above. More Li atoms on the outside sites of the graphene layer will be clustered because of the positive adsorption energy.

Meanwhile, we tested the specific capacity of the MoO<sub>2</sub>/G nanocomposite, since the average adsorption energy of the Li atoms on the outside sites of the MoO<sub>2</sub> layer is negative, we preferred to adsorb multiple layers of Li atoms on the outside sites of the MoO<sub>2</sub> layer. The geometric structures observed following the adsorption of 3 to 10 layers are shown in Fig. 4a–f. Each layer contains 25 Li atoms and it was found that the absolute value of the average adsorption energy decreased as the number of layers increased, as shown in Fig. 4g. The adsorption energy associated with the adsorption of ten layers of Li atoms is −0.278 eV, which means that more Li atoms could be adsorbed on the outside sites of the MoO<sub>2</sub> layer. So, we can conclude that the MoO<sub>2</sub>/G nanocomposite can increase the specific capacity of Li atoms.

We also calculated the theoretical gravimetric capacity of MoO<sub>2</sub>/G using the formula:  $C = nF/(M_{\text{MoO}_2/\text{G}} + nM_{\text{Li}})$ ,<sup>23</sup> where  $n$  is the number of adsorbed Li atoms and  $F$  is the Faraday constant (26 801 mA h mol<sup>−1</sup>),  $M_{\text{MoO}_2/\text{G}}$  and  $M_{\text{Li}}$  are the mole weights of the MoO<sub>2</sub>/G nanocomposite and Li atom. When adsorbing nine layers of Li atoms, the estimated total capacity is 1682 mA h g<sup>−1</sup>. Because the adsorption energy for nine layers of Li atoms is negative, we can conclude that the specific capacity of the MoO<sub>2</sub>/G nanocomposite will be larger than 1682 mAhg<sup>−1</sup>. Overall, the MoO<sub>2</sub>/G nanocomposite outperforms graphene and MoO<sub>2</sub> as an anode material for LIBs because of its higher capacity.

### 3.3 Electronic properties

The conductivity of LIBs plays an important role in the evaluation of electrode materials. In order to gain a deep understanding of the electronic properties, we calculated the projected density of states (PDOS) and the charge density difference of MoO<sub>2</sub>/G before and after Li adsorption, as shown in Fig. 5. As shown in Fig. 5a, because the energy bands of the MoO<sub>2</sub>/G nanocomposite shift due to electron transfer from graphene to MoO<sub>2</sub>, the d orbital of the Mo atom in MoO<sub>2</sub> and the p orbital of the C atom in graphene pass through the Fermi energy level. By comparing the PDOS of MoO<sub>2</sub>/G before and after Li adsorption, it is found that MoO<sub>2</sub>/G still retains its metallic properties, and that the d orbital of the Mo atom does not change much at the Fermi energy level. Thus, the MoO<sub>2</sub>/G nanocomposite, as an anode material for LIBs, has metallic properties and good conductivity. Conversely, when one Li atom is adsorbed in the interlayer, as shown in Fig. 5b, Li transfers charge with both the MoO<sub>2</sub> and graphene layers. Bader charge analysis shows that 0.867|e| is donated to MoO<sub>2</sub>

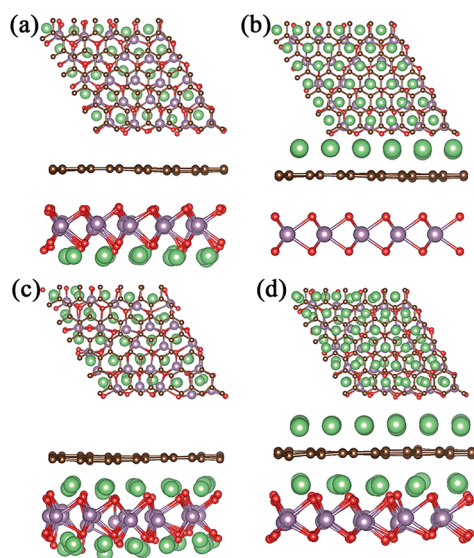


Fig. 3 Top and side views of the geometric structures observed following adsorption of different numbers of Li layers. (a) and (b) One-layer adsorption on the outside sites of the MoO<sub>2</sub> and graphene layers. (c) and (d) Interlayer and one-layer adsorption at the outside sites of the MoO<sub>2</sub> and graphene layers.





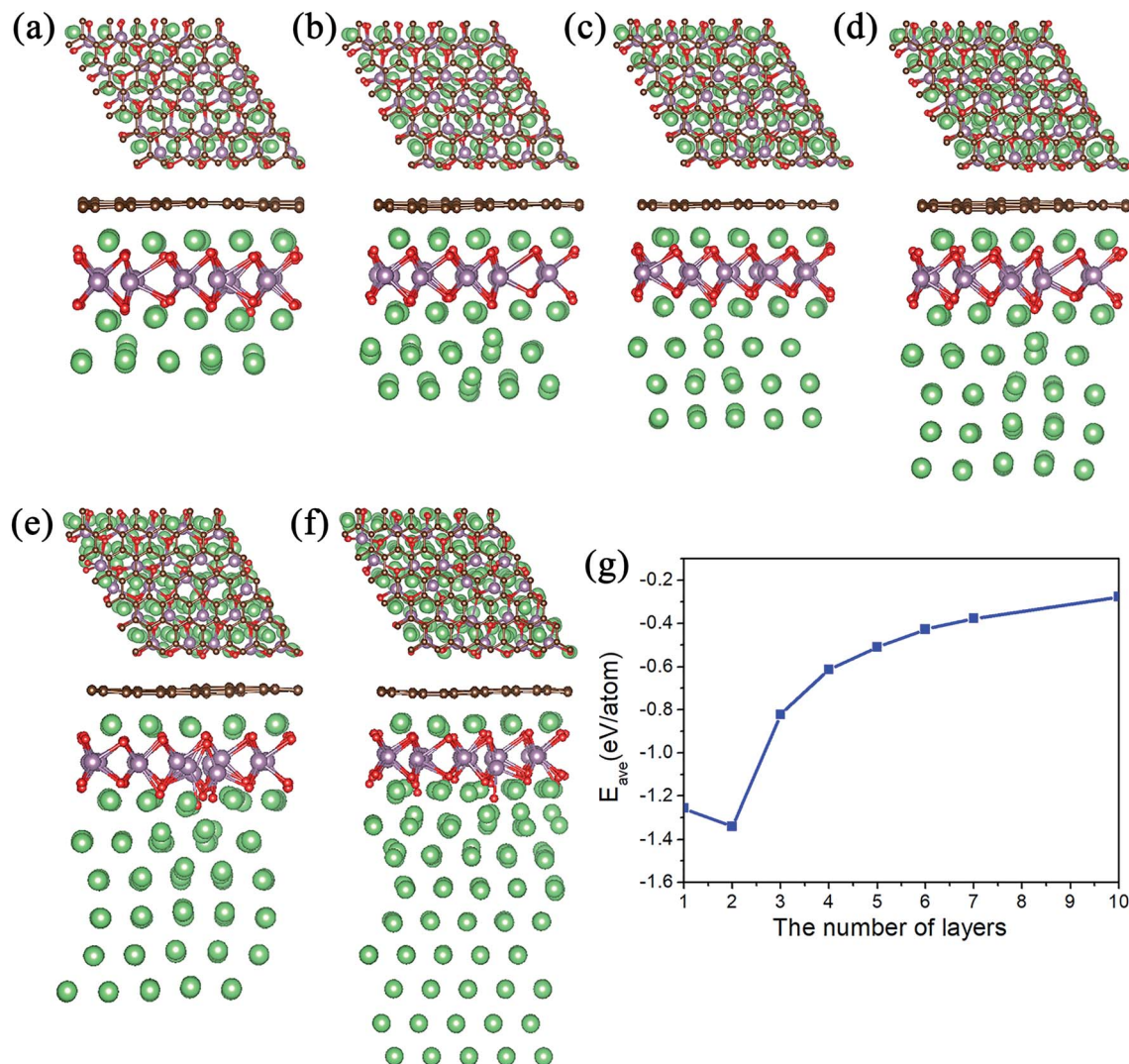


Fig. 4 (a)–(f) Top and side views of the geometric structures obtained as the number of Li adsorption layers on the outside of the MoO<sub>2</sub> layer is increased. (g) The changes in average adsorption energy with increasing Li atom layers.

and graphene. While one Li atom is adsorbed on the outside sites of the MoO<sub>2</sub> or graphene layers, as shown in Fig. 5c and d, charge transfer only occurs between the Li atom and either the MoO<sub>2</sub> or graphene layers. Bader charge analysis shows that 0.900|e| or 0.897|e| is donated to MoO<sub>2</sub> or graphene, respectively.

### 3.4 Diffusion properties

The charge/discharge rate of LIBS is closely related to the diffusion performance of Li atoms in the anode material. Therefore, we calculated the diffusion properties of Li atoms on the surface of MoO<sub>2</sub> and the MoO<sub>2</sub>/G nanocomposite. The Li atom diffusion paths are shown in Fig. 6. The calculation uses the NEB method to insert three coordinates between the two nearest adjacent stable Li atom adsorption sites. As shown in Fig. 6a–c, the diffusion energy barriers for a Li atom on the surface of pristine MoO<sub>2</sub> and on the outside sites of the MoO<sub>2</sub>/G nanocomposite are about 0.17 eV, 0.16 eV and 0.33 eV,

respectively. So, the diffusion energy barriers for a Li atom on the surfaces of the MoO<sub>2</sub>/G nanocomposite are smaller than those on the pristine materials (the energy barrier of pristine graphene is 0.37 eV (ref. 6 and 22)). However, when a Li atom diffuses in the MoO<sub>2</sub>/G interlayer, the energy barrier is no longer periodic and depends on the relative positions of the Li atom and MoO<sub>2</sub> and the C atom of graphene. As shown in Fig. 6d, the biggest energy barrier is up to 0.29 eV and the smallest one is 0.02 eV. Compared with the symmetric MoO<sub>2</sub>/G nanocomposites constructed by Ma,<sup>13</sup> the diffusion of Li atoms in the asymmetric structure is more favorable. Through the above results, it can be seen that the diffusion performance of Li atoms is improved after the nanocomposite is constructed. Therefore, we can conclude that LIBS that use the MoO<sub>2</sub>/G nanocomposite as the anode material are more conducive to charge transport and have a faster charge/discharge rate, which is in line with the experimental results.<sup>12</sup>



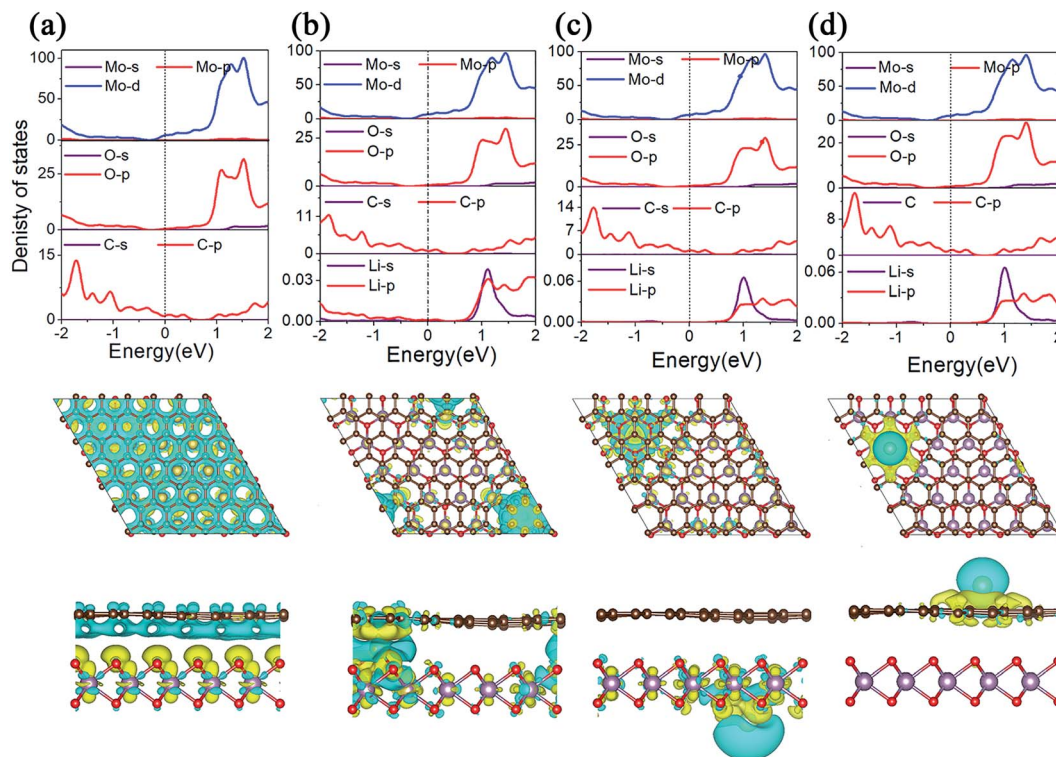


Fig. 5 (a) PDOS of MoO<sub>2</sub>/G and the charge density difference between MoO<sub>2</sub> and graphene. (b)–(d) PDOS of one Li atom adsorbed on different layers of MoO<sub>2</sub>/G and charge density differences between Li and the nanocomposite. The yellow region indicates electron accumulation, and the blue region indicates electron depletion.

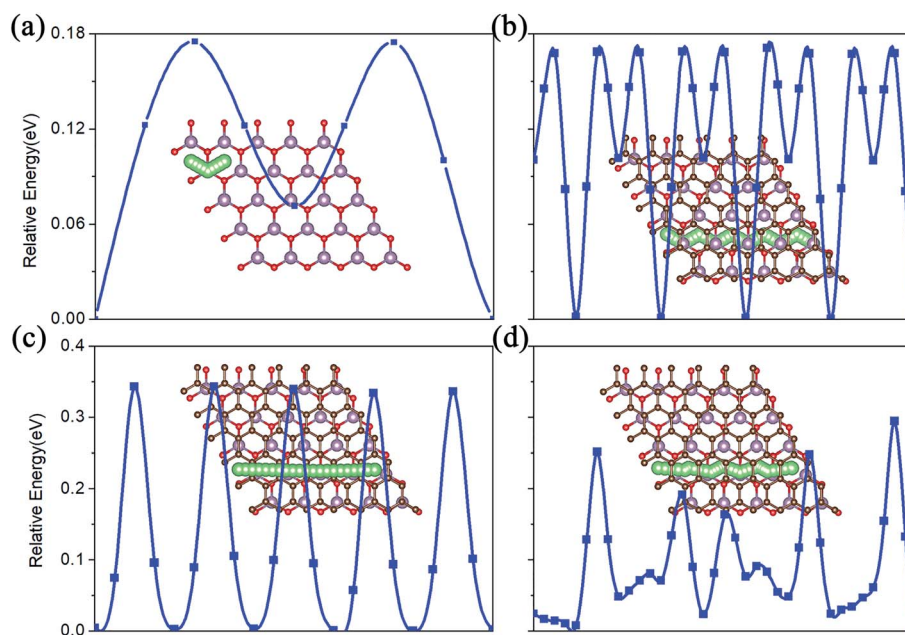


Fig. 6 The Li atom diffusion paths and energy barriers. (a) On pristine MoO<sub>2</sub>. (b) and (c) On the outside of the MoO<sub>2</sub> and graphene layers of the nanocomposite. (d) In the interlayer of MoO<sub>2</sub>/G.

## 4. Conclusions

Through first-principles calculations, we systematically studied the electronic and Li-diffusion properties of an asymmetric

MoO<sub>2</sub>/G nanocomposite. Our results show that the asymmetric MoO<sub>2</sub>/G nanocomposite has good stability and that Li atoms can be stably adsorbed in the interlayer and on the outsides of the nanocomposite without the occurrence of clustering.

Importantly, because of the charge transfer between MoO<sub>2</sub> and graphene, the asymmetric MoO<sub>2</sub>/G nanocomposite is metallic and has a small diffusion barrier which increases the conductivity of the MoO<sub>2</sub>/G nanocomposite. Moreover, the van der Waals interactions between MoO<sub>2</sub> and graphene will promote adsorption on the two outside layers and on the interlayer of the MoO<sub>2</sub>/G nanocomposite. The interlayer adsorption of Li atoms can further promote the adsorption of Li atoms on the outside sites of the MoO<sub>2</sub> layer, thus increasing the storage capacity. The theoretical specific capacity of the MoO<sub>2</sub>/G nanocomposite is larger than 1682 mA h g<sup>-1</sup>, which is much higher than that of graphene and MoO<sub>2</sub>. These results make MoO<sub>2</sub>/G an attractive LIBS anode material.

## Conflicts of interest

There are no conflicts to declare.

## Acknowledgements

This work is supported by the Fundamental Research Funds for the Central Universities (2652017333) and National Natural Science Foundation of China (Grant No. 11404294 and 51772279).

## References

- 1 B. Wang, J. S. Chen, H. B. Wu, Z. Wang and X. W. Lou, *J. Am. Chem. Soc.*, 2011, **133**, 17146–17148.
- 2 Z. Wang, Z. Wang, W. Liu, W. Xiao and X. W. Lou, *Energy Environ. Sci.*, 2013, **6**, 87–91.
- 3 Y. Gu, F. Wu and Y. Wang, *Adv. Funct. Mater.*, 2013, **23**, 893–899.
- 4 Q. Tang, Z. Shan, L. Wang and X. Qin, *Electrochim. Acta*, 2012, **79**, 148–153.
- 5 K. Persson, V. A. Sethuraman, L. J. Hardwick, Y. Hinuma, Y. S. Meng, A. van der Ven, V. Srinivasan, R. Kostecki and G. Ceder, *J. Phys. Chem. Lett.*, 2010, **1**, 1176–1180.
- 6 C. Uthaisar and V. Barone, *Nano Lett.*, 2010, **10**, 2838–2842.
- 7 L. Zhou, H. B. Wu, Z. Wang and X. W. Lou, *ACS Appl. Mater. Interfaces*, 2011, **3**, 4853–4857.
- 8 Y. Sun, *Am. Chem. Soc.*, 2011, **5**(9), 7100–7107.
- 9 L. Yang, L. Liu, Y. Zhu, X. Wang and Y. Wu, *J. Mater. Chem.*, 2012, **22**, 13148.
- 10 J. Nicks, J. Zhang and J. A. Foster, *Chem. Commun.*, 2019, **55**, 8788–8791.
- 11 Y. Liang, S. Yang, Z. Yi, X. Lei, J. Sun and Y. Zhou, *J. Mater. Sci. Eng. B*, 2005, **121**, 152–155.
- 12 A. Bhaskar, M. Deepa, T. N. Rao and U. V. Varadaraju, *J. Power Sources*, 2012, **216**, 169–178.
- 13 J. Ma, J. Fu, M. Niu and R. Quhe, *Carbon*, 2019, **147**, 357–363.
- 14 G. Kresse, *Phys. Rev. B: Condens. Matter Mater. Phys.*, 1996, **54**(16), 11169–11185.
- 15 J. P. Perdew, K. Burke and M. Ernzerhof, *Phys. Rev. Lett.*, 1996, **77**, 3865–3868.
- 16 G. Henkelman, B. P. Uberuaga and H. Jónsson, *J. Chem. Phys.*, 2000, **113**, 9901–9904.
- 17 X. Lian, M. Niu, Y. Huang and D. Cheng, *J. Phys. Chem. Solids*, 2018, 120.
- 18 F. A. Rasmussen and K. S. Thygesen, *J. Phys. Chem. C*, 2015, **119**, 13169–13183.
- 19 C. Ataca, H. Şahin and S. Ciraci, *J. Phys. Chem. C*, 2012, **116**, 8983–8999.
- 20 S. Gong and Q. Wang, *J. Phys. Chem. C*, 2017, **121**, 24418–24424.
- 21 H. J. Hwang, J. Koo, M. Park, N. Park, Y. Kwon and H. Lee, *J. Phys. Chem. C*, 2013, **117**, 6919–6923.
- 22 D. Das, S. Kim, K. R. Lee and A. K. Singh, *Phys. Chem. Chem. Phys.*, 2013, **15**, 15128–15134.
- 23 Q. Peng, K. Hu, B. Sa, J. Zhou, B. Wu, X. Hou and Z. Sun, *Nano Res.*, 2017, **10**, 3136–3150.

